

Characterization of sintered silicates for environmental barrier coating materials

Fan Jie Feng^a, Dong Heon Lee^a, Ji Yeon Park^b and Kee Sung Lee^{a,*}

^aSchool of Mechanical Systems Engineering, Kookmin University, Seoul, 02707, Korea

^bNuclear Materials Development Division, Korea Atomic Energy Research Institute, Daejeon, 34057, Korea

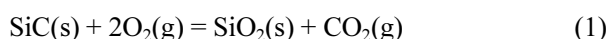
In this study, sintered silicates such as Yb₂SiO₅, Gd₂SiO₅, mullite, Ba-Sr-Al silicate (BSAS), and Y₂SiO₅ are fabricated and characterized. The oxide silicates are considered environmental barrier coating materials for protecting Si-based ceramic substrates in gas turbine applications from oxidation and corrosion resulting from reactions with water vapor at high temperature. Microstructure observation, phase analysis, and mechanical properties measurements indicate that the heat-treated Yb₂SiO₅ material includes crystalline phases, and it shows a relatively dense microstructure with improved mechanical properties.

Key words: Environmental Barrier Coating, Gas Turbine, Mechanical properties, Microstructure, Phase analysis, Rare-earth doped silicates.

Introduction

Similar to the combination of thermal barrier coatings (TBCs) and high-temperature alloy materials [1-3], the combination of environmental barrier coatings (EBCs) and silicate-based ceramic composites provides high-temperature-resistant components for gas turbines that effectively enhance the combustion temperature [4-8].

Silicate-based ceramic composites such as Si₃N₄, C/SiC-ceramic matrix composites (CMCs), and SiC/SiC-CMCs exhibit excellent mechanical properties at high temperature, e.g. excellent high-temperature strength and toughness [9-11]. In contrast to high-temperature alloys with an operating temperature of approximately 800 °C, the operating temperature of ordinary SiC/SiC-CMCs developed by Tyranno Corporation can reach 1200 °C and even 2000 °C, indicating that SiC/SiC-CMCs can withstand temperatures equal to or even higher than those of combinations of high-temperature alloys and thermal barrier coatings [12]. However, SiC-CMCs have a fatal weakness in that the silica on the surface is converted into a volatile silicon hydroxide species in the presence of high-temperature water vapor via the following reactions [13]:



These reactions cause the initiation of small cracks and

lead to the deterioration of the mechanical properties of the high-temperature-resistant structural components [14-15]. This problem can be solved by blocking the contact between the high-temperature vapor and the oxide layer on the surface of the SiC/SiC-CMCs by introducing EBC layers.

Similar to thermal barrier coatings, one of the main failures of EBCs stems from the mismatch of the thermal expansion coefficient (CTE) between the coating and the substrate layer. During gas turbine operation, different CTEs, different shrinkage rates, and residual stress may accumulate near the interface of the coating and substrate, which may lead to exfoliation of the EBCs [16-18]. Therefore, materials with CTEs similar to those of SiC/SiC-CMCs should be considered candidates for the coating. In this study, mullite, Ba-Sr-Al silicate (BSAS), and the rare-earth-doped silicates Gd₂SiO₅, Yb₂SiO₅, and Y₂SiO₅ were chosen as study materials because they not only have CTEs similar to those of SiC/SiC-CMCs but also excellent oxidation resistance. Coin samples prepared from these five materials were subjected to the same heat-treatment conditions. Afterwards, the most suitable EBC material was selected based on extensive investigation of their microstructure, phase structure, and mechanical properties.

Experimental procedure

Fabrication of coin samples by heat treatment

BSAS, whose chemical formula was Ba_{0.5}Sr_{0.5}Al₂Si₂O₈, was prepared from stoichiometric amounts of barium carbonate (BaCO₃, Kceracell Co., Ltd., Korea), strontium carbonate (SrCO₃, Kceracell Co., Ltd., Korea), alumina (Al₂O₃, Sumitomo Chemical Co., Ltd.,

*Corresponding author:
Tel : +82-2-910-4834
Fax: +82-2-910-4839
E-mail: keeslee@kookmin.ac.kr

Japan), and silicon oxide (SiO_2 , Kojundo Chemical Laboratory Co., Ltd.) powders in a molar ratio of 1 : 1 : 2 : 4. The corresponding mass fractions of the powders were weighed and placed in a polypropylene container, followed by the addition of an appropriate amount of alcohol. Then, Al_2O_3 balls with a diameter of 5 mm were added to the container and the powders were ball milled for 24 h in a ball mill machine (SBM-402A, Hansung Systems. Inc., Korea), affording a slurry of the powders. The slurry was dried at room temperature for 48 h and then placed in an oven at 80°C for 4 h. Finally, the agglomerate from the dried slurry was crushed in a mortar using a sieve machine, followed by filtering through an aperture less than $60\ \mu\text{m}$ in diameter, affording a BSAS mixed powder.

Yb_2SiO_5 and Gd_2SiO_5 powders were prepared similarly, following the same reaction conditions as for the BSAS preparation by mixing gadolinium oxide (Gd_2O_3 , 3N, Kojundo Chemical Laboratory Co., Ltd., submicron-sized particles) powder with silicon oxide (SiO_2 , Kojundo Chemical Laboratory Co., Ltd., particle size of $8\ \mu\text{m}$) powder and ytterbium oxide (Yb_2O_3 , 3N, Kojundo Chemical Laboratory Co., Ltd., submicron) powder with silicon oxide (SiO_2 , Kojundo Chemical Laboratory Co., Ltd., particle size of $8\ \mu\text{m}$) powder in a molar ratio of 1 : 1 to make slurries, which were dried under the same conditions as the BSAS powder to finally obtain the Gd_2SiO_5 and Yb_2SiO_5 samples. Y_2SiO_5 powder was also prepared from Y_2O_3 (5N, Hebei Pejin International Co. Ltd., particle size of $3\ \mu\text{m}$) and SiO_2 (VK-SP50, Xuancheng Jingrui New Material Co. Ltd., particle size of $0.6\ \mu\text{m}$).

The synthesized BSAS, Gd_2SiO_5 , Yb_2SiO_5 , and Y_2SiO_5 powders and the purchased mullite powder (DURAMUL 325F, Washington Mills, NY, U.S.A.) were weighed and pressed into coin samples. The molds containing the powders were pressed in a uniaxial pressing machine at a pressure of 50 MPa at room temperature for 40 s. Coin samples with a diameter of 25.4 mm and a thickness of 2-3 mm were obtained.

The coin samples prepared from the five materials were placed in a furnace and then heated in air to 1600°C at a heating rate of $5^\circ\text{C}/\text{min}$ for 10 h; they were then allowed to cool to room temperature. The ball-milled mixed powders, BSAS, Gd_2SiO_5 , and Yb_2SiO_5 , were first pre-heated at 1000°C for 2 h before heating at 1600°C to ensure chemical synthesis of the stoichiometric compounds. The experimental procedures are summarized in Fig.1.

Physical properties and load-displacement evaluation

The heat-treated coin samples were weighed using an electronic scale (GR-200, AND Co., Ltd., U.S.A) with an accuracy of 0.001 g to obtain their dry weights (dw). The coin samples were then placed in a beaker filled with almost boiling distilled water, which was heated

to maintain boiling, for 4 h to ensure that the distilled water thoroughly filled the internal cavities of the coin samples. Finally, the samples were removed from the beaker and the weight of samples in the pure water (dsu) and after wiping the water from their surfaces (dsa) was obtained. The accurate density of the heat-treated coin samples was calculated by the following equation:

$$\rho = \frac{dw}{dsa - dsu} \quad (3)$$

One surface of each dried coin sample was polished using a polishing machine (EcoMet-250, Buehler Co., Ltd., Hong Kong) for XRD experiments, which were performed within the range of 2θ from 0° to 80° . The other surface was gold coated using a gold-coating machine, and the surface microstructures of the five coin samples were characterized by field-emission scanning electron microscopy (FE-SEM, JEM-7610F, Jeol Ltd., Japan) at 200, 500, 1000, 2000, and $5000\times$ magnification. To test the mechanical behaviors of the five materials, the heat-treated coin samples were indented using a WC ball with a radius of 3.18 mm in a universal testing machine (Model No. 4467, Instron Co., Ltd., U.S.A) for load-displacement tests on the polished surfaces up to an indentation load, P , of 500 N at a rate of 100 N/min after a pre-test of 10 N.

Results and Discussion

The microstructures near the centers of the five heat-treated coin samples are shown in Fig. 2. The magnifications of the left and right images are $5000\times$ and $1000\times$, respectively. The porosity of the surface was analyzed by the ISO-Solution® software. Fig. 3 shows the porosity of the Yb_2SiO_5 , Gd_2SiO_5 , mullite, BSAS and Y_2SiO_5 coin samples. Simple visual observation of the images at $5000\times$ in Fig. 2 shows that the coin sample made from Yb_2SiO_5 exhibited a denser

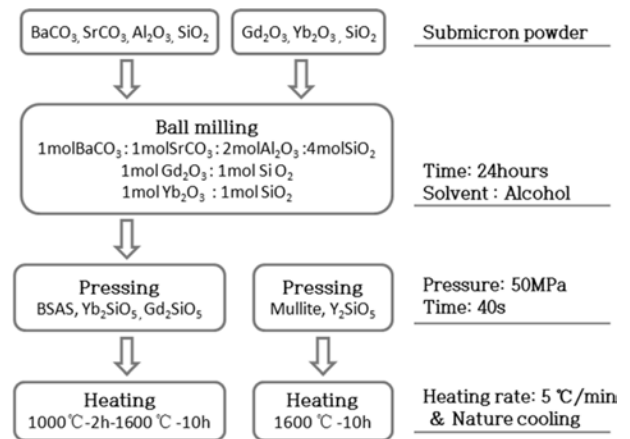


Fig. 1. Experimental procedures for fabrication of EBC materials in this study.

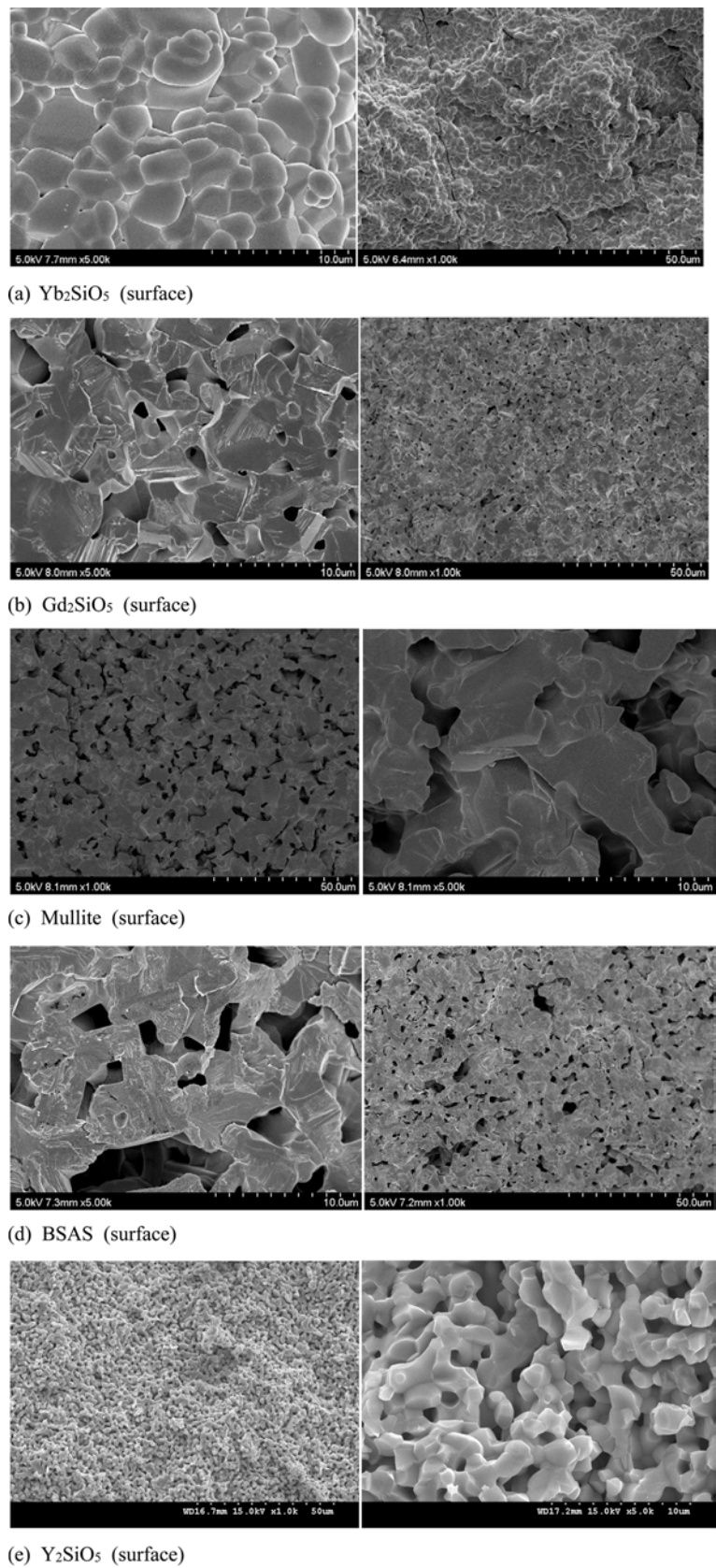


Fig. 2. SEM images (left: 1000 ×; right: 5000 ×) showing the microstructure of the surfaces of the coin samples: (a) Yb_2SiO_5 , (b) Gd_2SiO_5 , (c) Mullite, (d) BSAS, and (e) Y_2SiO_5 .

surface structure in comparison to the remaining four coin samples. For the remaining four coin samples,

according to the porosity analysis of the SEM images with a magnification of 1000× (shown in Fig. 3), the

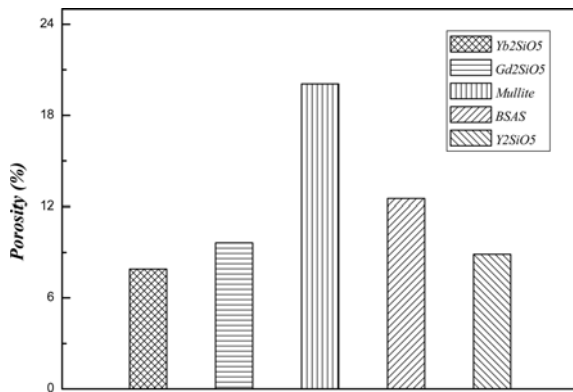


Fig. 3. Porosity of coin samples of Yb₂SiO₅, Gd₂SiO₅, Mullite, BSAS, and Y₂SiO₅.

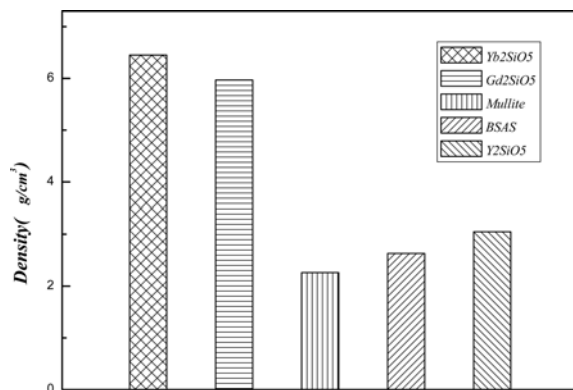


Fig. 4. Density of coin samples of Yb₂SiO₅, Gd₂SiO₅, Mullite, BSAS, and Y₂SiO₅.

surface porosities are in the following order: mullite (20.077%) > BSAS (12.515%) > Gd₂SiO₅ (9.632%) > Y₂SiO₅ (8.877%) > Yb₂SiO₅ (1.796%). Thus, both the microstructure observation and the accurate porosity analysis indicated that Yb₂SiO₅ exhibited the densest microstructure among the five heat-treated materials. Although the denser microstructure may lead to rapid thermal degradation upon multiple thermal cycling, the dense microstructure could effectively block the path of vapor into the substrate at high temperature and significantly reduce the contact probability between steam and the Si-based substrate. Therefore, Yb₂SiO₅ was considered the best EBC in terms of lower porosity.

Fig. 4 shows the density of the samples as measured by the Archimedes principle according to Eq. (3). According to the accurate density calculations, the order of densities of the five heat-treated coin samples is Yb₂SiO₅ (6.45 g/cm³) > Gd₂SiO₅ (5.97 g/cm³) > Y₂SiO₅ (3.05 g/cm³) > BSAS (2.63 g/cm³) > mullite (2.26 g/cm³). These results are mostly consistent with the FE-SEM observation and porosity analysis, further indicating that Yb₂SiO₅ exhibits the densest surface microstructure upon heat treatment at 1600 °C for 10 h.

Fig. 5 shows the XRD results of phase analysis of the five heat-treated coin samples. The XRD patterns of

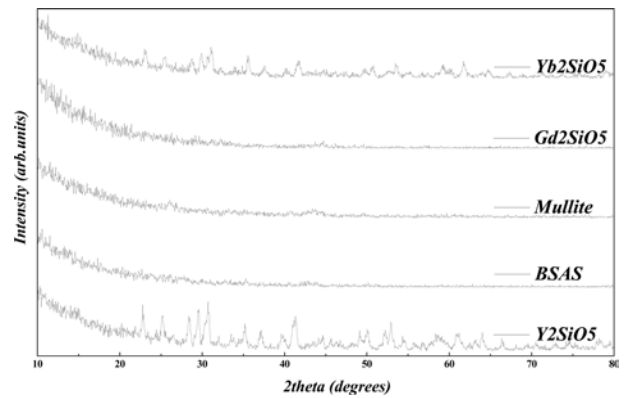


Fig. 5. XRD analysis of coin samples of Yb₂SiO₅, Gd₂SiO₅, mullite, BSAS, and Y₂SiO₅.

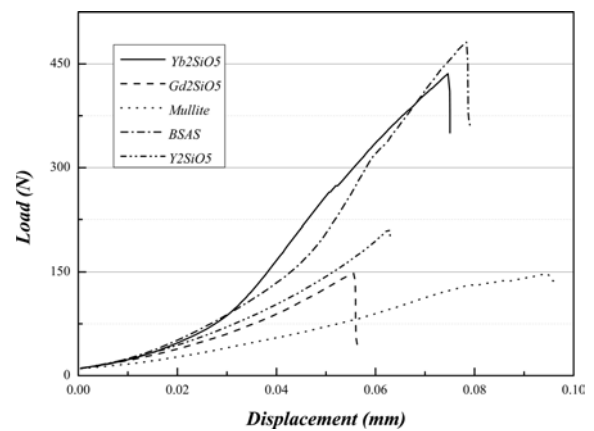


Fig. 6. Indentation load-displacement behavior of coin samples of Yb₂SiO₅, Gd₂SiO₅, mullite, BSAS, and Y₂SiO₅ at respective maximum load.

Gd₂SiO₅, mullite and BSAS did not show any obvious peak. These results indicate that these three materials did not form crystalline phases at temperatures < 1600 °C. On the other hand, crystalline peaks did appear in the XRD patterns for the Yb₂SiO₅ and Y₂SiO₅ coin samples. Although the intensity and location of the peaks show broadened peak, most of the peaks correspond to those of JCPDS cards. The result indicates that Yb₂SiO₅ and Y₂SiO₅ were successfully synthesized by heat treatment and desirable crystalline phases, which were detected as the EBC materials under the given experimental conditions. Although some references reported that the coating formed by Atmosphere Plasma Spray (APS) did not produce crystalline phases after sintering for certain times and temperatures, our results showed that crystalline phases were detected. When the amorphous phases are converted to crystalline phases, thermal expansion mismatch occurs, which in turn leads to failure of the coatings. Therefore, based on the XRD results of the five heat-treated materials, we expect EBCs prepared from Y₂SiO₅ and Yb₂SiO₅ by APS to form a stable crystalline phase. Relative to the coatings prepared from Yb₂SiO₅ and Y₂SiO₅, crystalline phases in

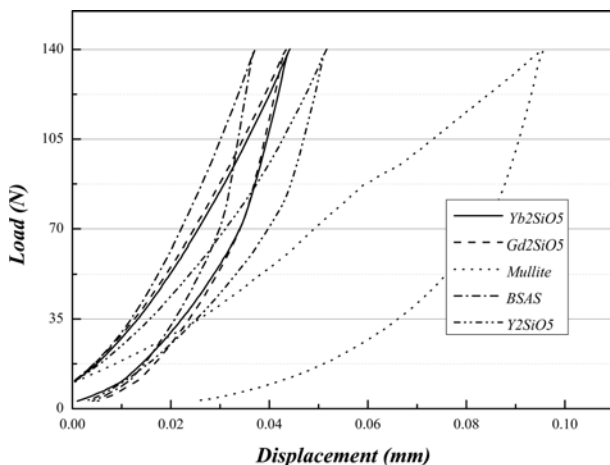


Fig. 7. Indentation load-displacement behavior of coin samples of Yb_2SiO_5 , Gd_2SiO_5 , mullite, BSAS, and Y_2SiO_5 at the load of $P = 140$ N.

mullite, Gd_2SiO_5 , and BSAS were not detected. It is thought that the coatings made from Yb_2SiO_5 and Y_2SiO_5 exhibit high density through the formation of a eutectic liquid during heat treatment and the formation of crystalline phases during cooling. During gas turbine operation, this feature of crystallinity can reduce the coating defoliation by thermal cycling, which is useful in extending the operating life of the EBCs.

In order to investigate the mechanical behavior of each EBC sample, the maximum loads of the five coin samples were determined using a load-displacement test with a contact load, P , of 500 N using a WC sphere with a radius of 3.18 mm. Figure 6 shows that the maximum loads were mainly concentrated in two regions, namely, BSAS and Yb_2SiO_5 showed maximum loads near 450 N, whereas Y_2SiO_5 , Gd_2SiO_5 , and mullite showed maximum loads near 150 N. Thus, the maximum load of BSAS and Yb_2SiO_5 was three times higher than that of the other three materials. Because the lowest maximum load among the five coin samples was 148 N (mullite), 140 N was selected as the maximum load for comparison of load displacement under the same load, and the results obtained by complete load-unload hysteresis curves are shown in Figure 7. The final displacement of mullite was 0.025 mm after unloading from 500 N, whereas the other four coin samples showed load displacements of less than 0.005 mm. For the test under a load of 140 N, the displacements are in the following order: BSAS (0.036 mm) < Yb_2SiO_5 and Gd_2SiO_5 (both 0.043 mm) < Y_2SiO_5 (0.05 mm) < mullite (0.095 mm). Comprehensive analysis from Figure 6 and Figure 7 indicates that BSAS and Yb_2SiO_5 exhibit better mechanical properties than the other three materials. Under the same impact, the EBCs prepared from BSAS and Yb_2SiO_5 are expected to show a longer operating life in terms of mechanical loadings.

Conclusions

The conclusions from analysis of the EBC materials by microstructure observation, phase analysis, and mechanical properties measurements are as follows:

1) The microstructure observation and porosity analysis indicate that Yb_2SiO_5 shows a comparably denser structure than the other materials. Although thermal degradation by the denser structure should be considered, it is expected that the dense structure could effectively block the contact between high-temperature steam and the substrate, and thus Yb_2SiO_5 with its highly dense surface is one of the best EBC candidate material in terms of microscopic structure.

2) The formation of crystalline phases reduces the possibility of a reaction with water vapor at high temperature owing to the lack of dimensional changes generated by the phase transition from an amorphous phase, thus extending the operating life of the coatings. The heat-treated Yb_2SiO_5 and Y_2SiO_5 materials, each of which formed a crystalline phase, were relatively good EBC materials.

3) The maximum load and load-unload curves of the five coin samples showed that BSAS and Yb_2SiO_5 have much better mechanical properties than the other three materials; therefore, these two materials were the best EBC materials in term of mechanical properties.

Finally, our results show that Yb_2SiO_5 is the best EBC material among the five materials owing to its excellent properties in terms of density, the presence of a crystalline phase, and load characteristics.

Acknowledgments

This work was supported by a Korea Evaluation Institute of Industrial Technology (KEIT) grant funded by the Korean government (MOTIE).

References

1. X.Q. Cao, R. Vassen, and D. Stoeber, *J. Eur. Ceram. Soc.* 24 (2004) 1-10.
2. Z.q. Sun, M.S. Li, and Y.C. Zhou, *J. Eur. Ceram. Soc.* 29 (2009) 551-557.
3. E. Garcia, P. Miranzo, and M.I. Osendi, *J. Therm. Spray. Techn.* 22[5] (2013) 680-689.
4. Z.Q. Sun, J.Y. Wang, M.S. Li, and Y.C. Zhou, *J. Eur. Ceram. Soc.* 28 (2008) 2895-2901.
5. Z.Q. Sun, Y.C. Zhou, and M.S. Li, *J. Mater. Res.* 23[3] (2008) 732-736
6. K.N. Lee, D.S. Fox, and N.P. Bansal, *J. Eur. Ceram. Soc.* 25 (2005) 1705-1715.
7. V. Herb, G. Couégnat, and E. Martin, *Composites: Part A.* 41 (2010) 1677-1685.
8. A. Aziz and R.T. Bhatt, *J. Compos. Mater.* 46[10] (2011) 1211-1218.
9. C.V. Cojocaru, D. Levesque, C. Moreau, and R.S. Lima, *Surf. Coat. Technol.* 216 (2013) 215-223.
10. S. Ramasamy, S.N. Tewari, K.N. Lee, R.T. Bhatt, and D.S.

- Fox, Surf. Coat. Technol. 205 (2010) 266-270.
11. K.N. Lee, Surf. Coat. Technol. 1[7] (2000) 133-134.
 12. J. Kimmel, N. Miriyala, J. Price, K. More, P. Tortorellib, H. Eatonc, G. Linseye, and E. Sun, J. Eur. Cerma. Soc. 22 (2002) 2769-2775.
 13. M.P. Brady, B.L. Armstrong, H.T. Lin, M.J. Lance, K.L. More, L.R. Walker, F. Huang, and M.L. Weaver, Scr. Mater. 52 (2005) 393-397.
 14. K.N. Lee, D.S. Fox, J.I. Eldridge, D. Zhu, R.C. Robinson, N.P. Bansal, and R.A. Miller, J. Am. Ceram. Soc. 86[8] (2003) 1299-1306.
 15. H. Wen, S. Dong, P. He, Z. Wang, H. Zhou, and X. Zhang, J. Am. Ceram. Soc. 90[12] (2007) 4043-4046.
 16. B.J. Harder and K.T. Faber, Scr. Mater. 62 (2010) 282-285.
 17. M. Aparicio and A. Duran, J. Am. Ceram. Soc. 83[6] (2000) 135-1355.
 18. C. Kim, Y.S. Heo, T.W. Kim, and K.S. Lee, J. Korean Ceram. Soc. 50[5] (2013) 326-332.